EQUATORIAL WAVES IN THE SATELLITE-OBSERVED CLOUD VELOCITY FIELD OVER THE PACIFIC

A THESIS SUBMITTED TO THE GRADUATE DIVISION OF THE UNIVERSITY OF HAWAII IN PARTIAL FULFILLMENT OF THE REQUIREMENTS FOR THE DEGREE OF

MASTER OF SCIENCE

IN OCEANOGRAPHY

MAY 1983

By
Lewis M Rothstein

Thesis Committee:

Gordon Groves, Chairman
Klaus Wyrtki
Brent Gallagher

We certify that we have read this thesis and that in our opinion it is satisfactory in scope and quality as a thesis for the degree of Master of Science in Oceanography.

Thesis Committee

Gordon Groves B.S.
Chairman

Brent Gallagher

Acknowledgements

I am grateful to Bernard Kilonsky for his indispensable help in understanding the cloud-velocity data, and for his many valuable suggestions. I also thank Colin Ramage, James Sadler and Klaus Wyrtki for their advice. This work was supported by the National Science Foundation through Grant Number OCE 77-17566.

Abstract

A space-time spectral analysis is applied to the 900 mb meridional wind component over the Equatorial Pacific Ocean. Cloud drift vectors, in the form of movie loops derived manually from cloud tracking satellites, constitute the data base for this investigation.

The major conclusions are as follows:

1) The maximum energy density levels of the wind occur at low wavenumbers over a broad range of frequencies. These disturbances appear to manifest themselves as fluctuations occurring simultaneously over a large span of longitude.

2) Investigation of the high frequency-high wavenumber structure is difficult due to the general shortage of reliable data and the uneven satellite sampling intervals. Selection of spectral parameters becomes a compromise between the problems of high aliasing and low reliability. A high frequency-low wavenumber (time lag of 5 hours and space separation of 2.1° longitude) study was selected.

3) There was no indication of a distinct 4-day signal in our spectra.

4) There appears to be less high-frequency energy in the equatorial band (1.05°S-1.05°N) than in the other two more southerly bands (5.25°S-3.15°S and 3.15°S-1.05°S).

TABLE OF CONTENTS

LIST OF FIGURES

LIST OF TABLES

I. Introduction

Knowledge of the large scale spatial and temporal structure of the tropical wind field is essential to our understanding of global ocean-atmosphere climatic variability as well as a variety of other oceanic and atmospheric processes. Recently, much attention has been focused on the description of the equatorial Pacific wind field [Barnett, 1977; Halpern, 1978; Wyrtki and Meyers, 1976]. In this region, the transport of heat by the equatorial ocean current system is dependent on the overlying wind field. Of course, the wind field is influenced by the oceanic heat budget thereby insuring a complex feedback system. The purpose of this paper is to describe, through the statistics of the energy spectrum, the frequency-wavenumber structure of the meridional component of the wind field over the eastern equatorial Pacific Ocean. Waves in only the east-west direction are considered. The initial impetus for this study was provided by results reported by Groves and Miyata [1967]. In that study, peaks in the sea-level spectrum of Canton Islands (2°49'S, 171°40'W) in the Phoenix Group at periods of four and five days were found to be coherent with the local meridional wind component. We were thus interested in verifying the existence of the four and five day signals from the present analysis. Wallace [1971] summarizes other pertinent literature on the 4-5 day wave being sought.

To study the large scale variability of the wind field, a satellite observational system must be used. Estimated low-level (900 mb) wind vectors from geostationary satellites have been derived since June 1969 from NASA's Application Technology Satellites ATS-1 and

ATS-3. These satellites relayed sequences of cloud position photographs to an earth receiving station. The photographs were then used to prepare a film loop displaying cloud motions for both cirrus level and cumulus, stratus level clouds. The operational procedures for estimating wind vectors from the film loops are described elsewhere [Young, Doolittle and Mace, 1972]. The launch of NASA's Synchronous Meteorological Satellite SMS-1 in May 1974 as part of NOAA's Geostationary Operational Environmental Satellite (GOES) program provided for the automatic extraction of low-level wind estimates by computer pattern matching. Cloud imaging for both manual and computer estimates is accomplished by a visible and infrared spin scan radiometer (VISSR), sensitive to both visible and infrared portions of the spectrum. Wind sets by computer pattern matching are generated by different techniques, one of which is described in Suomi [1975]. The present study utilizes the SMS-1 and the SMS-2 manual cloud photograph-movie loop data exclusively, from October 1974 to June 1977. Description of the data set is given in Section II.

There have been some questions as to the accuracy with which low-level cloud motion vectors represent the near-surface wind field, especially near the equator. Some of the editing procedures are suspect; for example, a cloud motion vector is accepted when deviations between it and the geostrophic wind derived from the previous 6-hourly surface analysis are less than 60° and 16 knots [Green, 1975; Young, 1975]. The use of geostrophy in editing cloud motion vectors casts some doubt as to the data's representativeness for near-surface winds near the equator. The uncertainty of the cloud's vertical position is

another cause of skepticism. Fortunately, confidence estimates are recorded for each cloud position recorded as well as for each velocity, thereby enabling the user to reject those uncertain wind vectors based on the confidence estimates. Confidence estimates were given as integers from 0 (lowest confidence) to 9 (highest confidence). Only data for which the analyst had the highest confidence of knowing both the level and velocity of the cloud were used in this study.

Beyond direct comparisons of independently measured winds [Halpern, 1978], the quality of satellite winds can be assessed through comparisons of the known dynamics of the wind field with features that are represented in the cloud-drift data. It is hoped that the results of this study will contribute information to aid us in the determination of the representativeness of cloud motions for the estimation of the low-level equatorial wind field.

II. Data

A low-level (900 mb) wind estimate is recorded at a position and at a time in which a low-level cloud is available for tracing, thereby rendering our data unevenly distributed in both space and time. All of the satellite wind estimates used in this study were derived from the film loop technique mentioned earlier. We were therefore limited to wind estimates during daylight hours only.

For this initial study, we have chosen to examine three latitude bands, each about 2° latitude wide. These latitude bands are 5.25°S-3.15°S, 3.15°S-1.05°S and 1.05°S-1.05°N (bands 1, 2 and 3 respectively). The longitudinal range of the study area is 80°W to 180° and the

temporal range is October 1974 to June 1977. All statistics and spectra contain no latitudinal structure information within a given latitude band.

The satellite wind estimates were obtained from a National Enviromental Satellite Service (NESS) tape containing all satellite derived low-level winds over the Pacific Ocean. The spatial and temporal distribution of the data, for each of the three latitude bands and the total of all three bands is illustrated in Figure 1.

The months of November 1974, April, June and August 1975 were missing from the NESS-tape. There were no data from October 1974 to March 1975 over the western part of the study area due to the absence of the SMS-2 satellite, which was launched in February 1975. The SMS-2 was positioned over the equator and 135°W to increase coverage over the Central Pacific Ocean. SMS-1 was initially positioned over the equator at 45°W and then moved 105°W, arriving there on February 16, 1976. The reason for the decaying data coverage from April 1976 to the end of the study period is that manually derived wind estimates were being phased out in lieu of estimates derived from computer pattern matching techniques.

This study is limited to the meridional component of the cloud drift velocities as it was found in previous studies [Groves, 1956] that the correlation between meridional wind and oceanic response (sea level) is simpler than for the zonal wind component. The mean and standard deviation of the satellite-estimated meridional wind speeds are given in Table 1.

	180°	170°W	160°W	150°W	140°W	130°W	120°W	110°W	100°W	90°W	80°W	Total
						1974						
Oct.	0	0	0	0	0	0	0	32	82	84	12	210
Dec.	0	0	0	0	0	0	14	35	27	11	0	87
						1975						
Jan.	0	0	0	0	0	0	12	30	14	9	1	66
Feb.	0	0	0	0	0	0	2	7	11	1	0	21
March	0	0	0	0	0	0	1	1	15	2	0	19
May	0	0	13	19	40	63	37	48	29	24	6	279
July	0	0	11	23	61	78	46	57	60	42	5	383
Sept.	0	0	14	58	88	124	59	94	56	26	1	520
Oct.	0	0	27	51	73	105	77	86	55	23	2	499
Nov.	0	0	18	39	55	72	55	50	55	39	2	385
Dec.	4	19	57	71	70	71	36	17	10	18	1	374
						1976						
Jan.	2	10	29	45	53	48	24	16	8	1	0	236
Feb.	4	10	32	44	55	51	18	15	2	5	2	238
March	0	6	11	19	20	13	9	5	3	2	0	88
April	0	3	3	4	9	7	8	3	0	0	0	37
May	0	2	0	4	3	7	4	3	0	0	0	23
June	0	3	2	4	7	5	10	5	12	4	0	52
July	1	1	5	1	5	5	12	11	6	11	0	58
Aug.	0	2	6	5	7	9	7	9	10	3	1	59
Sept.	1	0	3	3	7	0	0	2	1	1	0	18
Oct.	1	9	8	8	14	19	11	6	3	3	0	82
Nov.	2	5	7	8	5	9	7	9	5	2	0	59
Dec.	0	1	3	10	5	11	8	4	5	3	0	50
						1977						
Jan.	0	1	1	3	3	10	4	9	5	0	0	36
Feb.	0	0	6	9	9	13	4	2	2	4	0	49
March	0	0	6	6	3	7	1	2	0	2	0	27
April	0	1	3	6	12	23	11	9	5	5	2	77
May	0	2	2	9	6	8	7	2	6	1	0	43
June	0	1	4	6	9	6	5	5	6	1	0	43
Total	15	76	271	455	619	764	489	574	493	327	35	4118

(a)

	180°	170°W	160°W	150°W	140°W	130°W	120°W	110°W	100°W	90°W	80°W	Total
						1974						
Oct.	0	0	0	0	0	0	0	20	65	76	10	171
Dec.	0	0	0	0	0	0	5	16	20	7	2	50
						1975						
Jan.	0	0	0	0	0	0	7	21	19	7	1	55
Feb.	0	0	0	0	0	0	2	9	11	1	0	23
March	0	0	0	0	0	0	2	4	4	2	0	12
May	0	0	9	36	51	57	25	26	18	7	1	230
July	0	0	20	50	84	74	27	28	41	34	3	361
Sept.	0	0	27	86	93	125	63	69	50	18	1	532
Oct.	0	1	26	73	93	114	58	57	35	18	1	476
Nov.	0	0	13	25	62	87	33	45	37	29	5	336
Dec.	5	20	42	61	82	66	25	15	10	14	1	341
						1976						
Jan.	2	8	31	46	44	52	22	9	3	1	0	218
Feb.	3	12	33	37	57	68	21	9	3	4	0	247
March	0	4	21	30	15	16	6	1	0	1	1	95
April	0	1	6	3	19	10	10	6	2	1	0	58
May	0	1	1	2	9	5	2	1	2	1	0	24
June	0	2	2	6	8	5	10	4	7	6	0	50
July	0	1	12	4	8	10	9	6	5	2	1	58
Aug.	0	1	5	8	20	16	24	12	10	5	0	101
Sept.	0	2	5	4	3	3	2	4	2	0	0	25
Oct.	4	4	7	8	16	18	9	2	3	1	0	72
Nov.	2	2	4	5	4	8	8	4	7	3	0	47
Dec.	0	0	2	3	13	12	9	4	5	4	0	52
						1977						
Jan.	0	3	1	5	5	7	8	6	3	0	0	38
Feb.	0	1	4	2	10	8	4	4	3	3	0	39
March	0	0	4	6	8	8	2	2	2	2	0	34
April	2	5	6	19	13	26	6	3	4	3	0	87
May	0	0	2	8	4	7	4	3	3	5	1	37
June	0	4	8	12	6	9	9	5	5	2	0	60
Total	18	72	291	539	727	811	412	395	379	257	28	3929

(b)

Fig. 1. Distribution of satellite inferred, 900 m.b., cloud drift velocity data, Oct. 1974 to June 1977.
(a) Latitude band 1; (b) Latitude band 2; (c) Latitude band 3: (d) Composite of all 3 latitude bands.

	180°	170°W	160°W	150°W	140°W	130°W	120°W	110°W	100°W	90°W	80°W	Total
						1974						
Oct.	0	0	0	0	0	0	0	3	17	12	2	34
Dec.	0	0	0	0	0	0	0	5	9	8	0	22
						1975						
Jan.	0	0	0	0	0	0	2	15	9	5	0	31
Feb.	0	0	0	0	0	0	4	7	9	2	0	22
March	0	0	0	0	0	0	1	7	5	4	1	18
May	0	0	9	13	24	18	6	8	3	3	0	84
July	0	0	9	26	38	26	8	12	10	3	1	133
Sept.	0	0	17	59	59	47	30	28	20	0	0	260
Oct.	0	1	12	47	56	56	31	23	10	2	2	240
Nov.	0	0	9	18	45	52	22	26	30	14	1	217
Dec.	0	9	19	47	52	37	22	11	7	9	0	213
						1976						
Jan.	0	8	8	21	26	22	10	5	2	0	0	102
Feb.	2	3	25	40	32	45	15	5	1	2	0	170
March	0	5	15	12	9	4	4	1	0	0	0	50
April	0	4	1	10	6	6	6	3	0	0	0	36
May	0	2	1	8	6	0	1	2	0	0	0	20
June	0	1	0	3	3	2	7	6	5	1	0	28
July	0	0	2	1	3	3	9	1	1	0	1	21
Aug.	0	0	2	6	11	15	4	2	2	0	0	42
Sept.	1	2	1	3	2	1	4	0	1	0	0	15
Oct.	1	6	4	9	6	11	6	1	2	0	0	46
Nov.	0	1	3	12	3	10	5	3	5	1	1	44
Dec.	0	0	0	5	5	7	3	4	4	8	1	37
						1977						
Jan.	0	0	0	1	1	2	1	4	1	0	0	10
Feb.	0	2	0	1	2	1	1	0	1	2	0	10
March	0	1	0	3	3	1	1	0	0	1	0	10
April	0	4	7	18	9	14	4	0	0	3	0	59
May	0	0	0	1	3	0	0	1	0	1	1	7
June	0	1	1	2	5	4	3	5	5	2	1	29
Total	4	50	145	366	409	384	210	188	159	83	12	2010

(c)

	180°	170°W	160°W	150°W	140°W	130°W	120°W	110°W	100°W	90°W	80°W	Total
						1974						
Oct.	0	0	0	0	0	0	0	55	164	172	24	415
Dec.	0	0	0	0	0	0	19	56	56	26	2	159
						1975						
Jan.	0	0	0	0	0	0	21	66	42	21	2	152
Feb.	0	0	0	0	0	0	8	23	31	4	0	66
March	0	0	0	0	0	0	4	12	24	8	1	49
May	0	0	31	68	115	138	68	82	50	34	7	593
July	0	0	40	99	183	178	81	97	111	79	9	877
Sept.	0	0	58	203	240	296	152	191	126	44	2	1312
Oct.	0	2	65	171	222	275	166	166	100	43	5	1215
Nov.	0	0	40	82	162	211	110	121	122	82	8	938
Dec.	9	48	118	179	204	174	83	43	27	41	2	928
						1976						
Jan.	4	26	68	112	123	122	56	30	13	2	0	556
Feb.	9	25	90	121	144	164	54	29	6	11	2	655
March	0	15	47	61	44	33	19	7	3	3	1	233
April	0	8	10	17	34	23	24	12	2	1	0	131
May	0	5	2	14	18	12	7	6	2	1	0	67
June	0	6	4	13	18	12	27	15	24	11	0	130
July	1	2	19	6	16	18	30	18	12	13	2	137
Aug.	0	3	13	19	38	40	35	23	22	8	1	202
Sept.	2	4	9	10	12	4	6	6	4	1	0	58
Oct.	6	19	19	25	36	48	26	9	8	4	0	200
Nov.	4	8	14	25	12	27	20	16	17	6	1	150
Dec.	0	1	5	18	23	30	20	12	14	15	1	139
						1977						
Jan.	0	4	2	9	9	19	13	19	9	0	0	84
Feb.	0	3	10	12	21	22	9	6	6	9	0	98
March	0	1	10	15	14	16	4	4	2	5	0	71
April	2	10	16	43	34	63	21	12	9	11	2	223
May	0	2	4	18	13	15	11	6	9	7	2	87
June	0	6	13	20	20	19	17	15	16	5	1	132
Total	37	198	707	1360	1755	1959	1111	1157	1031	667	75	10057

(d)

Fig. 1. Continued.

Table 1. Statistics of satellite-estimated meridional wind speeds, 900 mb level. (Averages over temporal and spatial extent of the study area for all three latitude bands.)

Latitude Band	Mean (m/sec)	Standard Deviation (m/sec)
5.25°S-3.15°S	1.90	3.42
3.15°S-1.05°S	1.93	3.45
1.05°S-1.05°N	1.73	3.48

III. Frequency-Wavenumber Analysis

a. Method of Analysis

In order to examine the characteristic time and space scales of the equatorial meridional wind field, a time-space power spectral analysis of the cloud motion data has been made. Let v(x,t) be the magnitude of the meridional component of the satellite derived wind in a given latitudinal band, a function of longitude x and time t. The apparent autocovariance function (R) can then be defined as

$$R(\eta,\tau) = \langle v(x,t)\, v(x+\eta, t+\tau)\rangle = R(-\eta,-\tau);\ -T<\tau<T,\ -L<\eta<L \qquad \text{(III-1)}$$

where brackets indicate averaging over both x and t, η is the longitude separation, τ is the time lag and T and L are the temporal and spatial extent of the data, respectively, R is seen to be independent of x and t, because we have assumed stationarity in both space and time. Also, ergodicity is implicit as it is hoped that simple time and space averaging will provide information about the underlying process and not just give information about the finite piece of record. Because we have assumed ergodicity (of which stationarity is a necessary assumption), we have eliminated the need for collecting an ensemble of records for the statistical description of the cloud velocity field.

To obtain estimates of the true power spectrum, we need to Fourier transform R. We applied a cosine (hanning) data window to R in order to reduce sideband energy. Tapering with cosine window was performed in both lag and separation space.

Let

$$H_\tau = \tfrac{1}{2}\left(1 + \cos\frac{\pi\tau}{\tau_m}\right)$$

$$H_\eta = \tfrac{1}{2}\left(1 + \cos\frac{\pi\eta}{\eta_m}\right) \qquad \text{(III-2)}$$

represent the "hanning," where τ_m is the maximum lag and η_m is the maximum separation employed in the formulation of R.

The frequency-wavenumber (σ-χ) spectrum is then defined as

$$S(\chi,\sigma) = \mathrm{Re}\left\{\iint R(\eta,\tau) H_\tau H_\eta \exp i(\chi\eta + \sigma\tau)\, d\eta\, d\tau\right\} \qquad \text{(III-3)}$$

$$= \iint R(\eta,\tau) H_\tau H_\eta \cos(\chi\eta + \sigma\tau)\, d\eta\, d\tau$$

For future computational procedures, following the development used by Munk, Snodgrass and Gilbert [1964], it will be useful to introduce the mixed quantity

$$C(\eta,\sigma) = \int R(\eta,\tau) H_\tau \exp(i\sigma\tau)\, d\tau$$

$$= \int R(\eta,\tau) H_\tau \cos(\sigma\tau)\, d\tau + i\int R(\eta,\tau) H_\tau \sin(\sigma\tau)\, d\tau \qquad \text{(III-4)}$$

$$= C_R(\eta,\sigma) + i\, C_I(\eta,\sigma)$$

Then the spectrum can be redefined as

$$S(\chi,\sigma) = \int C(\eta,\sigma) H_\eta \exp(i\chi\eta)\, d\eta$$

$$= \int C_R(\eta,\sigma) H_\eta \cos(\chi\eta)\, d\eta - \int C_I(\eta,\sigma) H_\eta \sin(\chi\eta)\, d\eta \qquad \text{(III-5)}$$

At this point we may also note the following symmetry relations:

$$S(\chi,\sigma) = S(-\chi,-\sigma)$$

$$C_R(\eta,\sigma) = C_R(\eta,-\sigma) = C_R(-\eta,\sigma)$$
$$C_I(\eta,\sigma) = -C_I(\eta,-\sigma) = -C_I(-\eta,\sigma) \qquad \text{(III-6)}$$

For the actual computations, the integrals are replaced by summations. Let us define time lag and longitude separation increments, $\Delta\tau$ and $\Delta\eta$ respectively. Then

$$\tau = i\,\Delta\tau \quad , \quad i = -m, \ldots, 0, \ldots, +m$$
$$\eta = j\,\Delta\eta \quad , \quad j = -\ell, \ldots, 0, \ldots, +\ell \qquad \text{(III-7)}$$

where m and ℓ are integers denoting the maximum lag and separation used in the analysis. In accordance with the intervals of Equations (III-7), the frequency and wavenumber increments are given by

$$\Delta\sigma = 2\pi/(2m+1)\Delta\tau \quad ; \quad \Delta\kappa = 2\pi/(2\ell+1)\Delta\eta . \qquad \text{(III-8)}$$

We also set

$$\sigma = q\Delta\sigma = 2\pi q/(2m+1)\Delta\tau \; ; \; q = -m, \ldots, 0, \ldots, +m$$

and (III-9)

$$\kappa = r\Delta\kappa = 2\pi r/(2\ell+1)\Delta\eta \; ; \; r = -\ell, \ldots, 0, \ldots, +\ell$$

From this point hence, we will be concerned with positive time lags only, i.e. i, q = o, ..., m. The negative time lag half-plane can be obtained from the symmetry relation (III-6). On the other hand, we will want to retain both positive and negative spatial separations, due to the important directional information (eastward and westward traveling energy) inherent in the definitions.

We are now ready to reformulate the spectral relationships in discrete form. From Equation (III-4) and the symmetry of R,

$$C_R(\eta,\sigma) = \Delta\tau\left\{R(\eta,0) + \sum_{i=1}^{m}\left[R(\eta,i\Delta\tau) + R(-\eta,i\Delta\tau)\right]\frac{1}{2}\left[1+\cos\left(\frac{2\pi i}{2m+1}\right)\right] * \right.$$

$$\left. * \cos\left(\frac{2\pi i q}{2m+1}\right)\right\} \qquad \text{(III-10)}$$

and

$$C_I(\eta,\sigma) = \Delta\tau\left\{\sum_{i=1}^{m}\left[R(\eta,i\Delta\tau) - R(-\eta,i\Delta\tau)\right]\frac{1}{2}\left[1+\cos\left(\frac{2\pi i}{2m+1}\right)\right] * \right.$$

$$* \sin\left(\frac{2\pi i q}{2m+1}\right) \qquad \text{(III-10a)}$$

The frequency-wavenumber spectrum, Equation (III-5), can then be computed from

$$S(\kappa,\sigma) = \Delta\eta\left\{C_R(0,\sigma) + 2\sum_{j=1}^{\ell} C_R(j\Delta\eta,\sigma)\frac{1}{2}\left[1+\cos\left(\frac{2\pi j}{2\ell+1}\right)\right] * \right.$$

$$\left. * \cos\left(\frac{2\pi j r}{2\ell+1}\right) - 2\sum_{j=1}^{\ell} C_I(j\Delta\eta,\sigma)\frac{1}{2}\left[1+\cos\left(\frac{2\pi j}{2\ell+1}\right)\right]\sin\left(\frac{2\pi j r}{2\ell+1}\right)\right\},$$

$$r = -\ell, \ldots, 0, \ldots, +\ell$$

$$\sigma \geq 0$$

(III-11)

The energy density spectra were computed from Equations (III-10) and (III-11). For all spectra in this paper, we have used m = 59 and ℓ = 19, resulting in real values of maximum time lag and space separation of 59 $\Delta\tau$ and 19 $\Delta\eta$. We are therefore calculating (m+1)(2ℓ+1) = (60)(39) = 2340 separate values of the energy density $S(\kappa,\sigma)$ for each spectrum. (It will be seen later that the selection of $\Delta\tau$ and $\Delta\eta$ will be such that the maximum lag and separation are much smaller than the

total time and space scales of the study, thus reducing the variance of the spectral estimates.) The energy density over the 39 x 60 (κ,σ)-matrix constitutes the principal result of this paper.

b. Estimation of the Autocovariance

In each of the three latitude bands the longitude separation η and time difference τ for every pair of v values were examined. For cases in which the values of (η,τ) lie within the maximum values considered, the product of the corresponding pair of v values is accumulated into a running sum $R(\eta,\tau)$ of such products for which $j\Delta\eta$, $i\Delta\tau$ is nearest to the actual values (η,τ). After all products have been accumulated, each sum is divided by the number of products contributing to that sum to provide an estimate of the average value of the product. The variance of the autocovariance function is discussed in the appendix. It is evident that the more products in each sum the greater will be the accuracy of the estimate. Also, the greater the values of $\Delta\eta$ and $\Delta\tau$, the larger will be the number of products in each sum. But the larger the values of $\Delta\eta$ and $\Delta\tau$, the smaller will be the folding wavenumber and folding frequency and, consequently, the larger will be the amount of aliased energy. It is thus seen that selection of these parameters is a compromise between confident statistics and low aliasing.

The high frequency-low wavenumber analyses discussed in Section (IIId) seemed to offer the best compromise in the selection of $\Delta\eta$, $\Delta\tau$. Basically, this indicates that there is so much high-frequency and high-wavenumber noise in the data that the amount of existing cloud-velocity data are barely sufficient to allow one to make a

statistically-significant estimate of spectral energy.

Due to the necessity of examining higher frequency signals (to relieve the aliasing), and even though a large longitudinal separation increment was used (for higher statistical reliability), some of the values of the autocovariance matrix $R(\eta,\tau)$ were formed from very few product pairs, i.e. there were large data gaps at certain lag-separation intervals. We therefore modified R according to the following prodecure. The largest lagged product value should be $R(o,o)$, the variance. If any $R(\eta,\tau)$ is greater than $R(o,o)$ or less than $-R(o,o)$, that value is replaced by $R(o,o)$ or $-R(o,o)$. Approximately 4% of R was modified in this way for latitude band 1.

The stability of the modified R (η,τ) estimates can be examined by looking at the distribution of numbers of products used in estimating $R(\eta,\tau)$. The distribution is illustrated in Figure 2 for latitude band 1. A continuous record would show a solitary spike at N_{max}, i.e. at N for $R(o,o)$. If the data were more evenly distributed with respect to longitude separation and time lag, the statistical reliability of the poorer $R(\eta,\tau)$ estimates. The smoothing could be accomplished by either employing an interpolative scheme to our raw velocity data or smoothing the modified R values directly. Both alternatives seem to accomplish the same goal, i.e. improved statistics of our spectra, but smoothing the modified R values requires less computational effort. For those estimates based on a number of products less than a preselected minimum n_m, the estimates are replaced by averages of products over a larger range of time lag and longitude separation (in the actual case, over a range of $3\Delta\tau$ and $3\Delta\eta$).

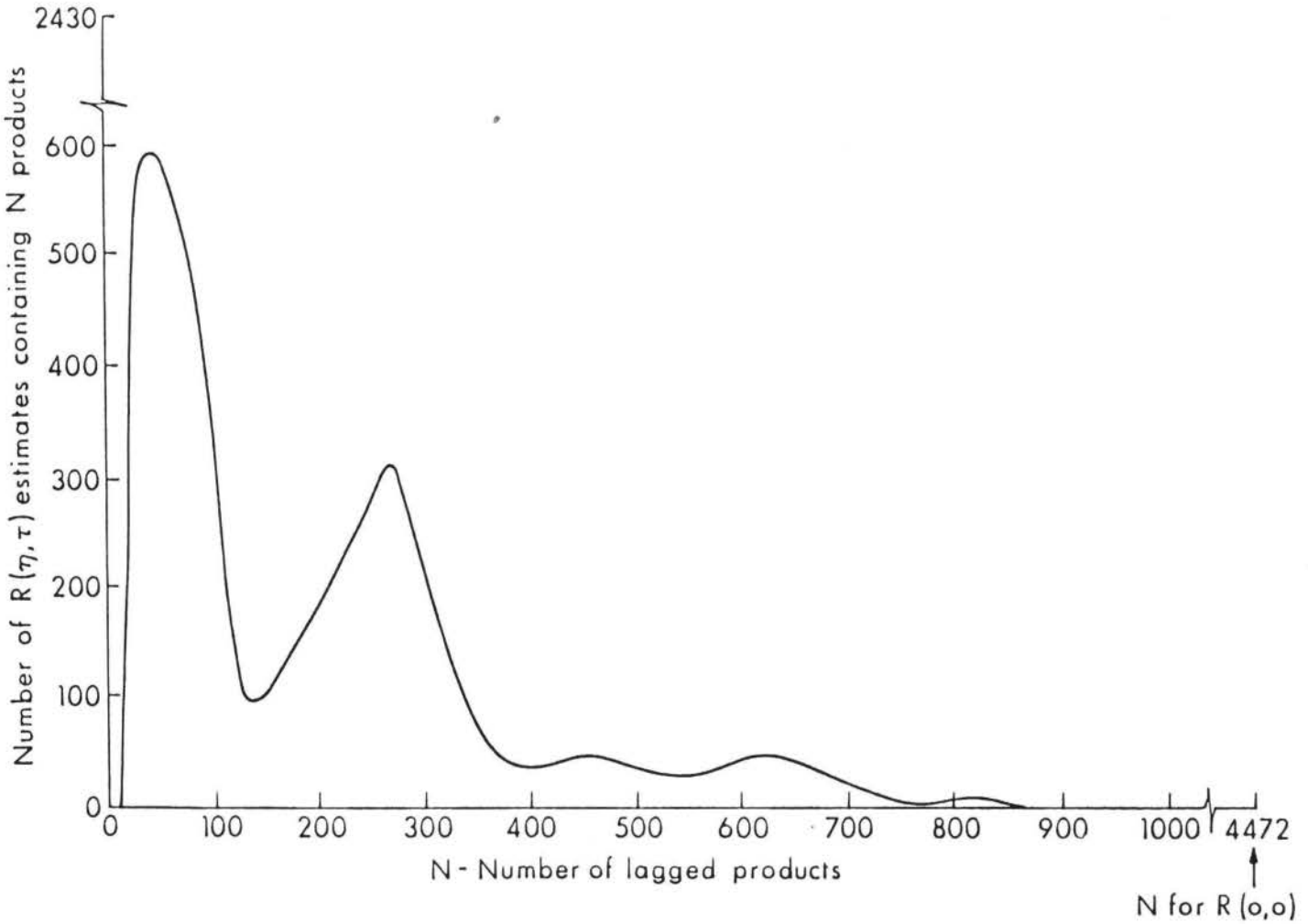

Fig. 2. Measure of the goodness of the apparent autocovariance function.

This is essentially a smoothing operation carried out with a two-dimensional boxcar kernel. The consequence of this smoothing operation, besides enhancing the reliability of the poorer estimates of $R(\eta,\tau)$, is to reduce the spectral energy in the higher frequencies and wavenumbers. If the smoothing kernel were applied over the entire (η,τ) domain it would represent a usual low-pass linear filter, and the effects are complicated and so no such compensation was attempted. The reader is just cautioned that the spectral values for the higher frequencies and wavenumbers, approaching the folding values, are somewhat too low, depending on the value n_m selected.

Three levels of smoothing have been arbitrarily chosen. The levels are n_m = 50, 175 and 350. For a smoothing of 50, for example, an individual modified R estimate composed of 50 products or less is replaced by a smoothed value. The reduction in the variance of the spectral estimates produced by the different smoothing levels will be illustrated.

c. High-frequency, high-wavenumber analysis

This study was carried out with $\Delta\tau$ = 5 hours and $\Delta\eta$ = 0.3°, giving folding frequencies of .1 cph and 1.67 cycle/degree. These values were selected on the basis of a preliminary study at lower frequencies and wavenumbers (higher values of $\Delta\tau$ and $\Delta\eta$) which seemed to indicate aliasing problems. The present study, with admittedly too small values of $\Delta\tau$ and $\Delta\eta$ to insure adequate statistical reliability, was made to roughly delineate the distribution of spectral density in order to assist in the selection of parameters for a study that would

be adequate in view of both the aliasing and statistical problems. The energy density spectrum for latitude band 1 is shown in Figure 3. The mean error of the spectral estimates in Figure 3 is 18 x 10^2 m^2 sec^{-2}/ $hour^{-1}$ $degree^{-1}$. This value represents the square root of the variance of each individual spectral estimate of the 39 x 60 matrix. Clumps of high energy values are, of course, more significant than are the individual values and thus the broad energy density highs of Figure 3 seem to be significant. A variance matrix of 39 x 60 values was computed for Figure 3 and all other spectra reported here. The matrix of variance was extremely flat at the mean variance level, hence the justification in basing our confidence estimates on the mean value of the variance. The computational formulae as well as a discussion of the statistical significance of the spectra presented in the paper are given in the Appendix.

From Figure 3, most of the energy density appears to reside in very low wavenumber regions at a variety of frequencies. Table 2 presents values of the energy, $\iint S(\kappa,\sigma)\, d\kappa d\sigma$, for each of the four specified regions. Region I defines the area under study in our preliminary low frequency-wavenumber analysis, which is seen to encompass an inadequate portion of the entire energy to insure sufficiently low aliasing error. The total energy, from a separate analysis of this region alone, was found to be 8.35 m^2 sec^{-2}. Comparison of this number with the energy found in Region I (see Table 2) indicates high levels of aliasing. From Figure 3, we can see that, for latitude band 1, most of this aliased energy is coming from the higher frequencies, rather than the higher wavenumbers. This is also verified

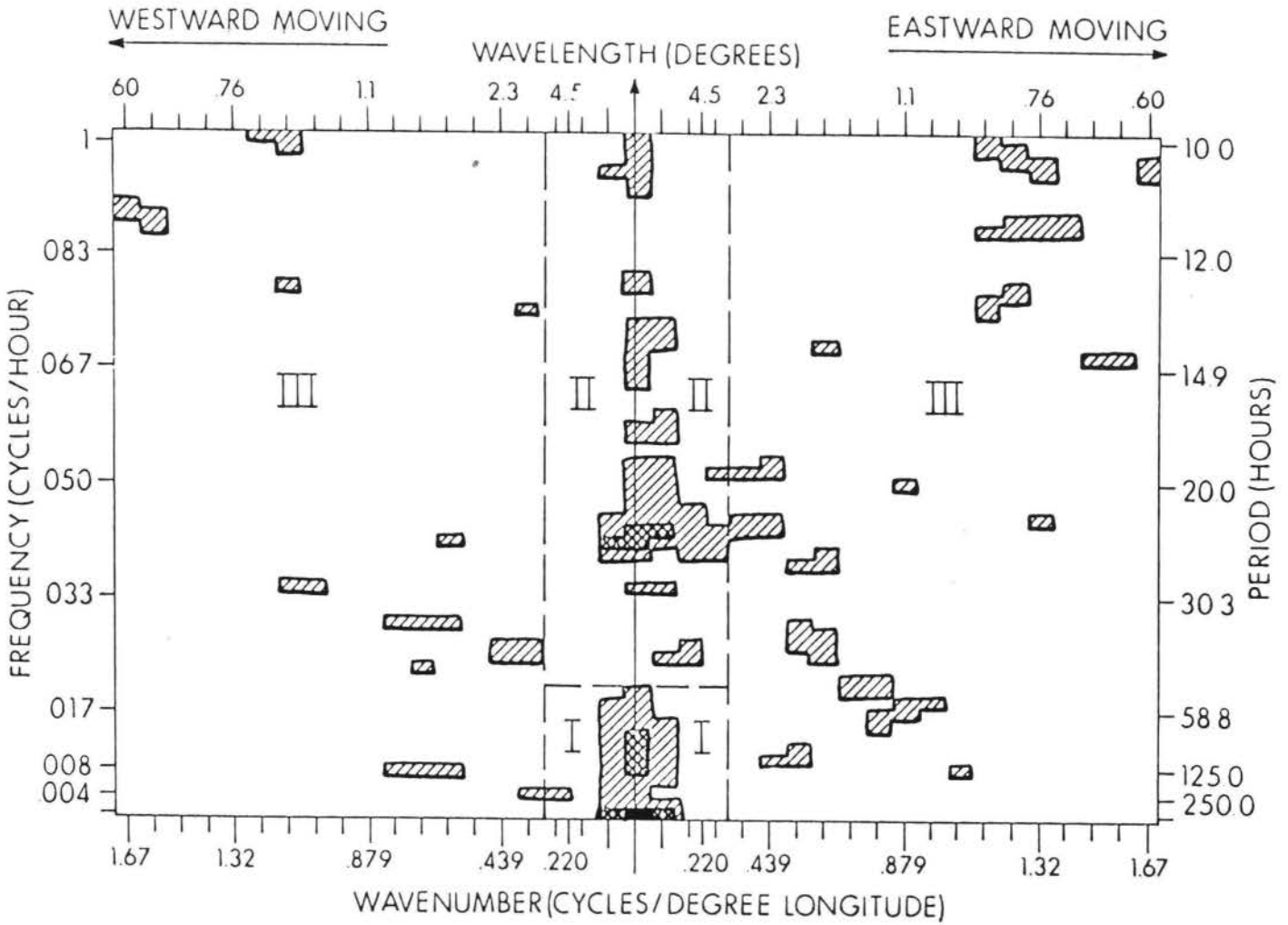

Fig. 3. High frequency-wavenumber energy density spectrum (m^2 sec^{-2}/$hour^{-1}$ $degree^{-1}$) of meridional velocity component at 900 m.b., latitude band #1. Successive shadings range from an energy density of 5000 (darkest), 500 and 100 (lightest). Roman numerals refer to separate study regions, described in the text. The mean error of an individual spectral estimate is 18×10^2 m^2 $sec^{-2}/hour^{-1}$ deg^{-1}.

Table 2. Energy, $m^2\ sec^{-2}$, of the regions I, II, and III depicted in Fig. 3

Region	Energy
I	3.86
II	3.54
III	1.67

by the low energy level in Region III. Thus, the results of Figure 3 guide us in selecting high frequency-low wavenumber parameters for future studies. (The energy in Region I + II, the region we are about to analyze, is approximately 80% of the total energy.) This result enables us to somewhat alleviate the problem of aliasing without incurring overwhelming statistical uncertainty.

d. High frequency-low wavenumber analysis

The primary results of this paper will be extracted from the high frequency-low wavenumber spectral analysis of the estimated satellite wind data. We choose $\Delta\tau$ = 5 hours and $\Delta\eta$ = 2.1° longitude, giving folding frequencies of .1 cph and .238 cycles/degree. Frequency resolution is thus 1.67×10^{-3} cph and wavenumber resolution is 1.25×10^{-2} cycles/degree.

The most striking feature about the frequency-wavenumber structure of the satellite estimated meridional wind velocity in this latitude band is the apparent lack of structure, except for one important feature (see Fig. 4). There appear to be high energy density levels at low wavenumbers at a variety of frequencies. This indicates fluctuations in the wind field that are simultaneous over long spans of longitude. The mean error of an individual estimate is high; however, the same comments expressed about the errors of the high frequency-wavenumber analysis apply here, that large areas of high energy density levels appear to be statistically significant.

The effects of smoothing on the energy density spectrum is to dramatically reduce the mean error for all smoothing levels (each smoothing level is applied to the original unsmoothed modified R, i.e.

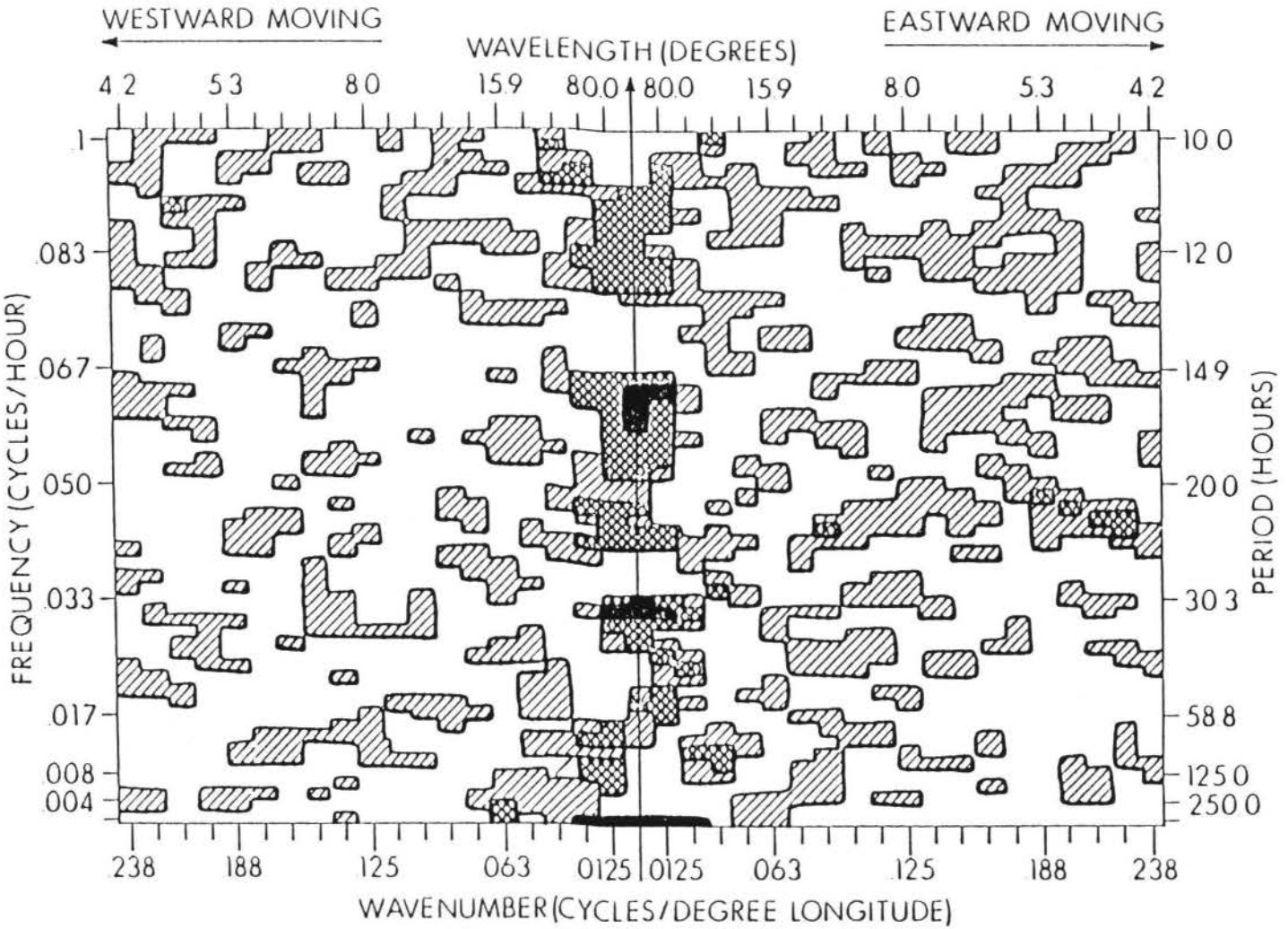

Fig. 4. High frequency-low wavenumber energy density spectrum (m^2 sec^{-2}/$hour^{-1}$ $degree^{-1}$) of meridional velocity component at 900 m.b., latitude band #1. Successive shadings range from an energy density of 5000 (darkest), 1000 and 200 (lightest). The mean error of an individual spectral estimate is 3400 m^2 sec^{-2}/$hour^{-1}$ deg^{-1}.

the smooth 50 level is not further smoothed to level 175, etc.). The "smooth spectra" are illustrated in Figures 5 through 7.

In all smoothed spectra (as well as the unsmoothed spectrum) there appears a diurnal peak at wavenumbers indicating eastward-moving activity as well as at a variety of other wavenumbers. As the error estimates are based on randomly distributed product contributions to the covariances they will overestimate confidence at frequencies near the diurnal, because of the lack of nighttime observations, and thus it is difficult to draw conclusions regarding this diurnal peak. Major spectral features throughout the smoothing process are conserved, lending confidence to the method. In Figure 7 an interesting feature emerges. There appears to be a variety of disturbances moving with different phase velocities eastward but all with approximately the same group velocity of about 2000 km/day. However, the dominant features throughout all levels of smoothing is the high energy density at low wavenumbers, disturbances that appear to manifest themselves as fluctuations occurring simultaneously over a large span of wavenumbers through the entire frequency range examined.

For economic reasons, the frequency-wavenumber spectra for latitude bands 2 and 3 were obtained for smoothing to level 175 only. The spectra are illustrated in Figures 8 and 9. The modification of R for latitude band 2 affected 3.5% of the R matrix. The equatorial band needed the largest modification, where 4.7% of R was modified. Again, we observe the high energy density levels at low wavenumbers throughout the frequency range examined as well as the higher diurnal energy density. As the equator is approached (band 3), we observe

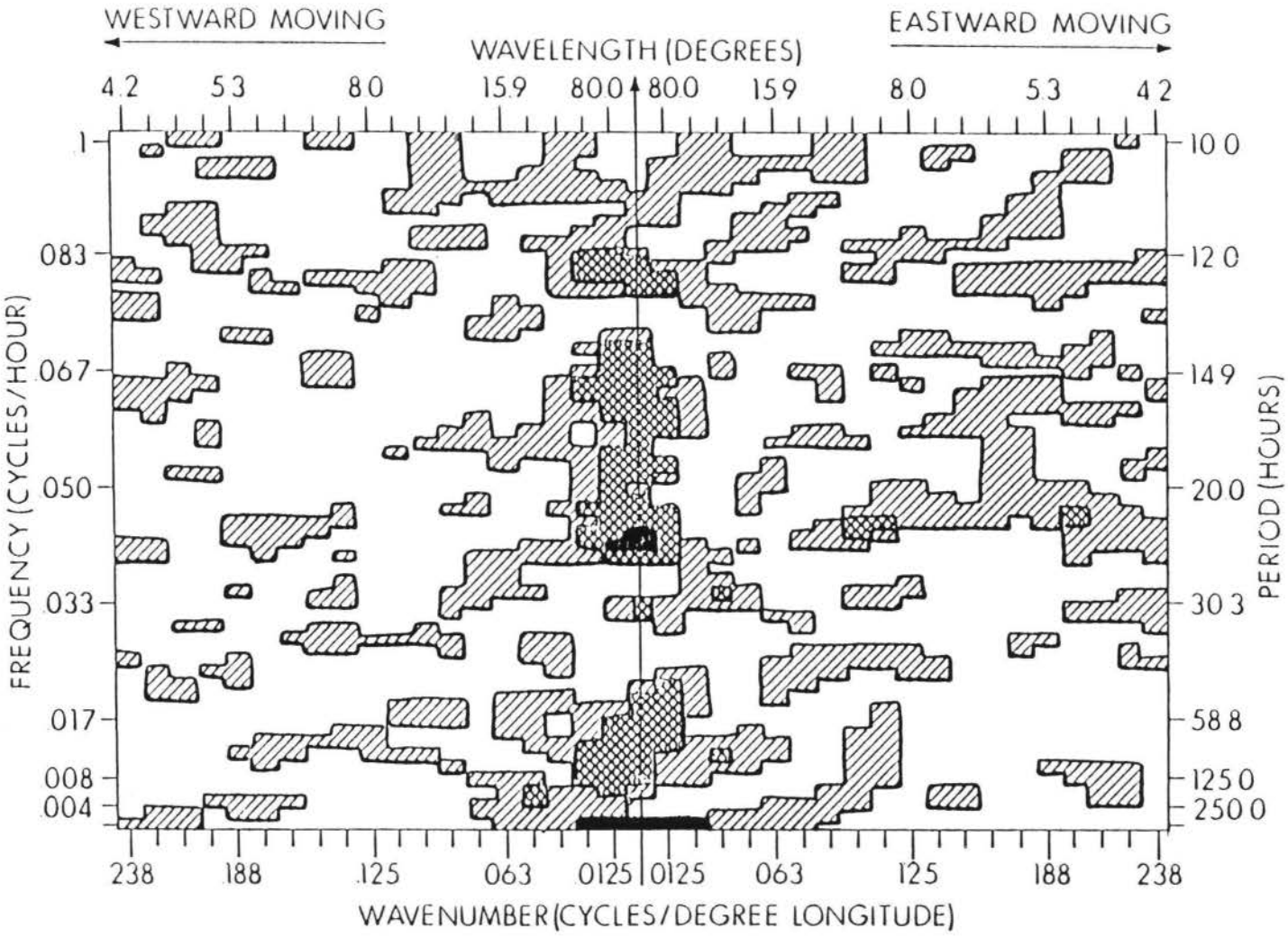

Fig. 5. Same as Fig. 4 except smoothing to level N=50. The mean error of an individual spectral estimate is reduced to 500 m^2 sec^{-2}/$hour^{-1}$ $degree^{-1}$.

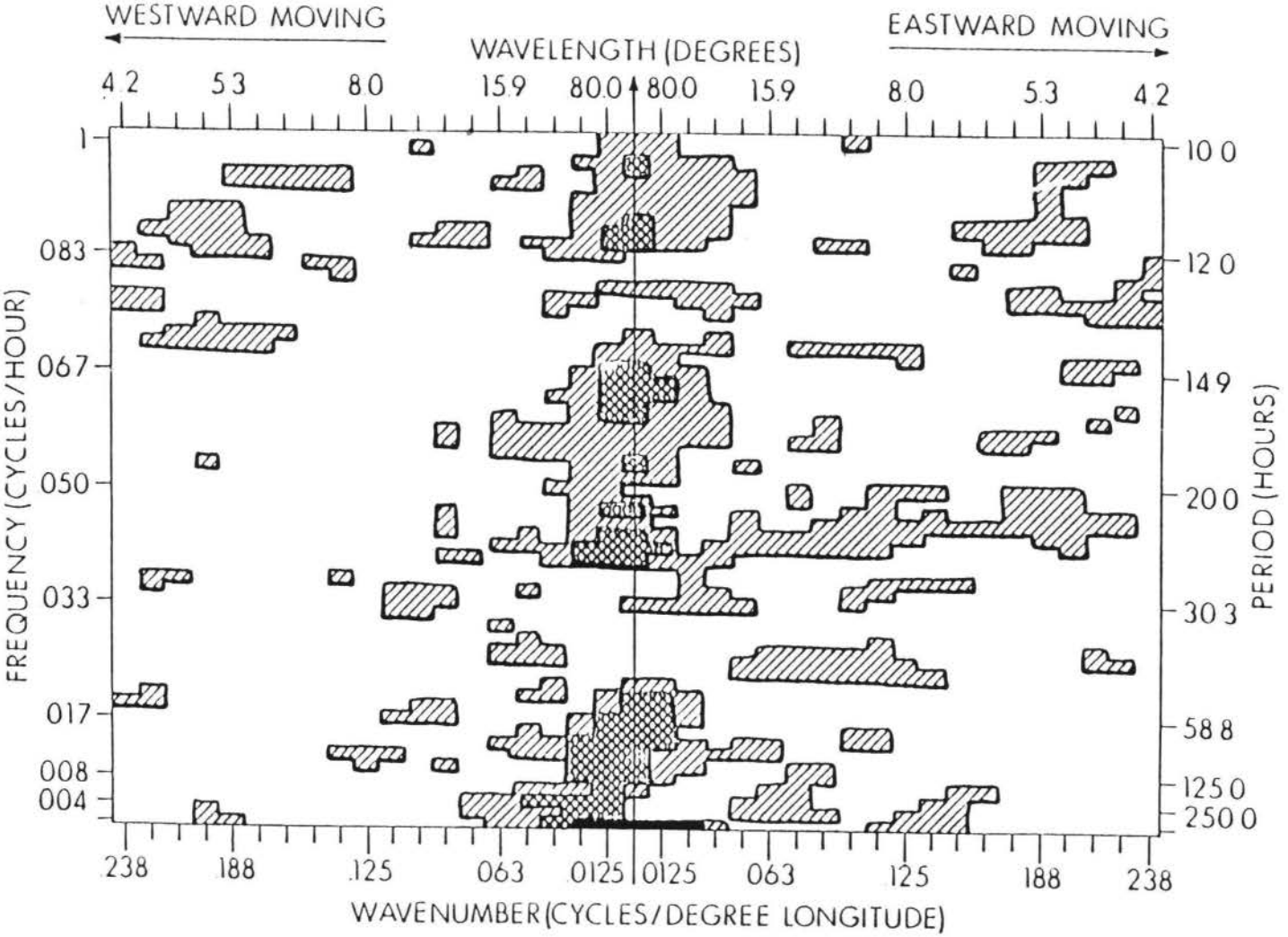

Fig. 6. Same as Fig. 4 except smoothing to level N=175. The mean error of an individual spectral estimate is reduced to 400 m^2 sec^{-2}/$hour^{-1}$ $degree^{-1}$.

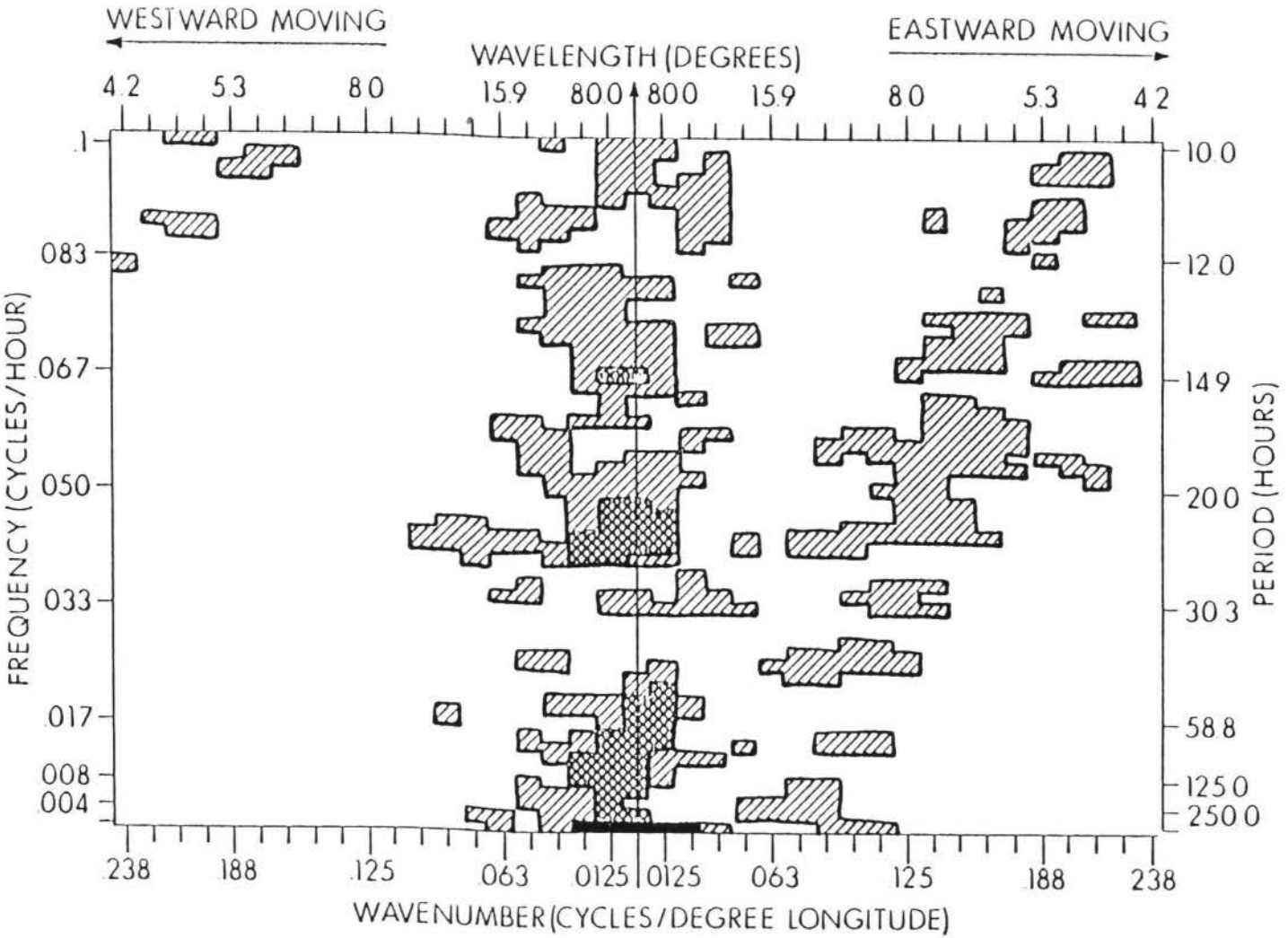

Fig. 7. Same as Fig. 4 except smoothing to level N=350. The mean error of an individual estimate is reduced to 300 m^2 sec^{-2}/$hour^{-1}$ $degree^{-1}$.

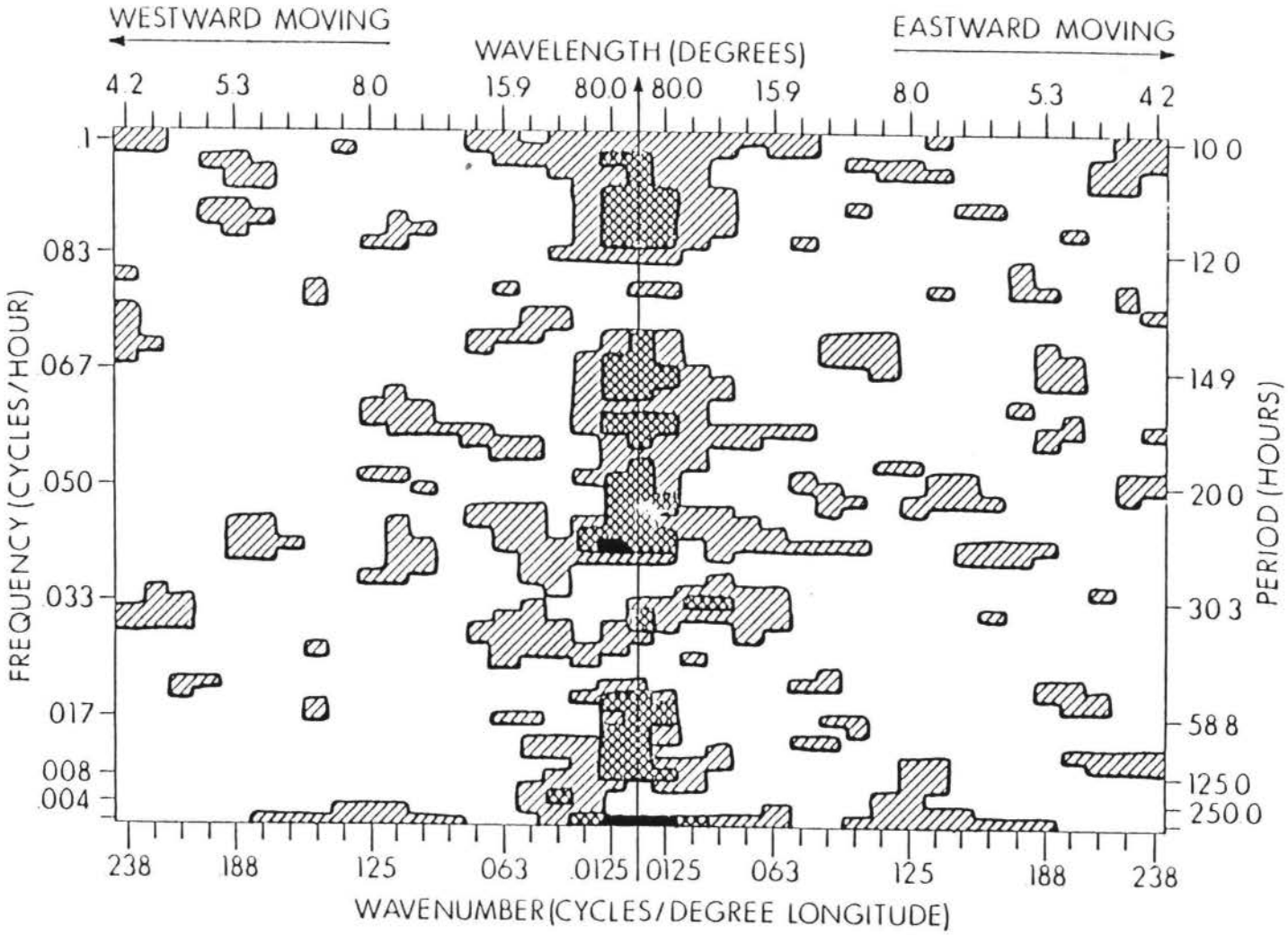

Fig. 8. Same as Fig. 4, latitude band #2. Spectra shown was smoothed to level N=175. The mean error of an individual spectral estimate is 400 m^2 sec^{-2}/ $hour^{-1}$ $degree^{-1}$.

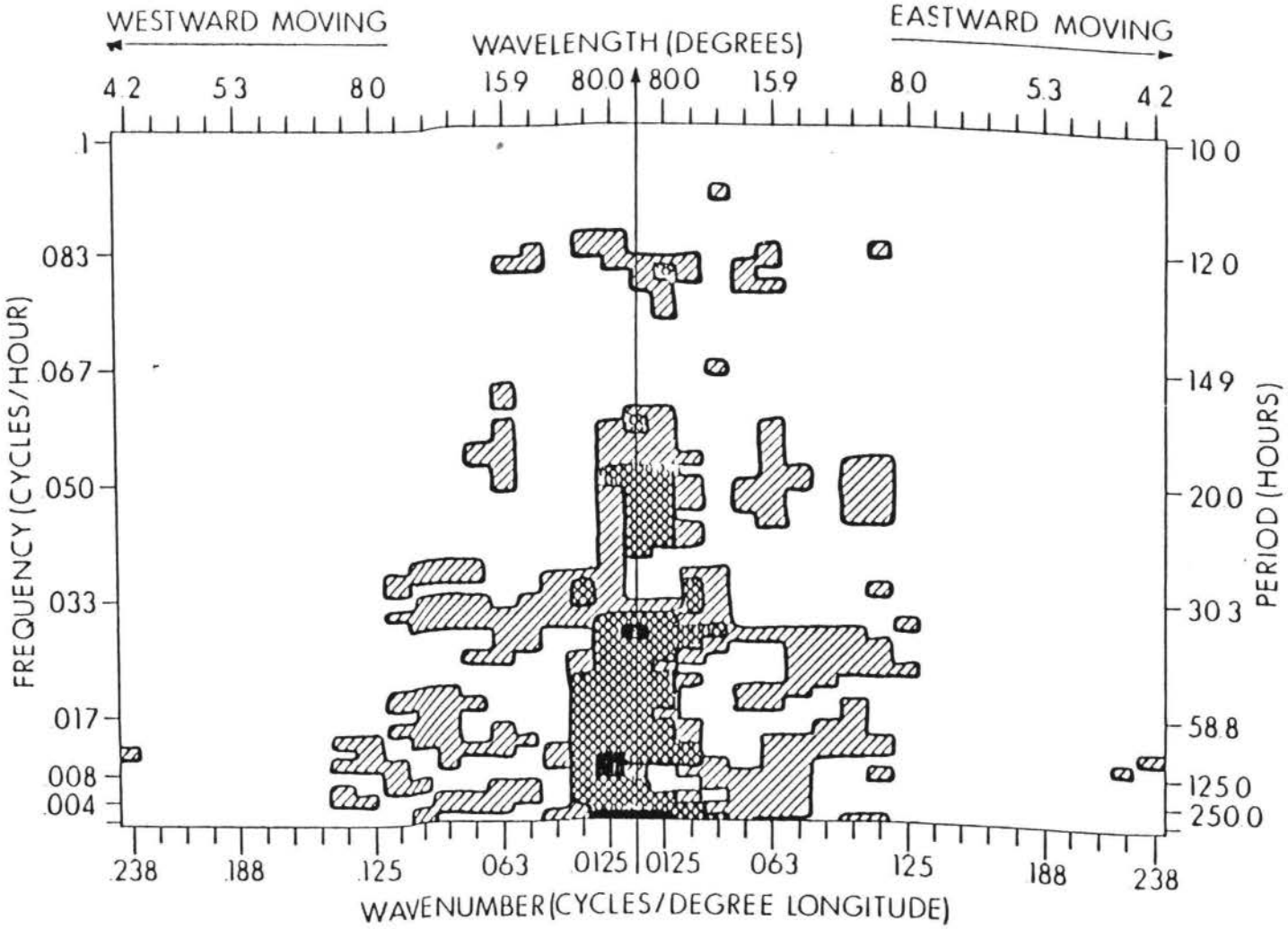

Fig. 9. Same as Fig. 4, latitude band #3 (equatorial band). Spectra shown was smoothed to level N=175. The mean error of an individual spectral estimate is 700 m^2 sec^{-2}/$hour^{-1}$ $degree^{-1}$.

less low wavenumber energy density at the higher frequencies than was present in the two more southerly latitude bands. Latitude bands 1 and 2 also show an energy density minimum at a period of approximately 10 days for low wavenumbers. Finally, we observe similarities in latitude bands 1 and 2 but as the equator is approached, the meridional wind structure changes significantly. This appears to be a reflection of the data sparsity in the equatorial latitude band.

A check of our results is provided by the fact that we must conserve energy at each step (raw data → a modified R → spectral estimates) of our analysis, except for loss of spectral energy due to the smoothing procedure described in Section IIIb. Table 3 presents such data for each of the three latitude bands. We see that the formation of the modified R leads to the expected dimunition of spectral energy. Otherwise there appears to be satisfactory agreement with the variously computed total energy value.

We can identify a small 4 and 5 day "peak" in the equatorial band at low wavenumbers although no such peak is evident in the two southerly latitude bands. The energy density in surrounding frequencies is approximately the same as the "peak" thus the significance of these periodicities is questionable. It has been suggested that I might turn my attention to latitude bands further south and also investigate the regions immediately north of our study area with the idea that perhaps the 4-day signal is generated more dominantly in these regions forcing the oceanic response at a distance (Colin Ramage, private communications).

Finally, I would like to briefly compare the magnitudes of our

Table 3. Energy conservation check. The energy derived from the spectra are for smoothed spectra at the 175 level. Units are m/sec.

Lat. Band	RMS Velocity from Raw Data	$\sqrt{R(o,o)}$	$\sqrt{\iint S(\kappa,\sigma)\,d\sigma\,d\kappa}$
1	3.91	3.91	3.02
2	3.95	3.96	3.24
3	3.88	3.85	3.12

energy densities with those of Halpern (1978). The energy density of Halpern's satellite inferred low-level winds at a frequency of .02 cph for the region 0°, 125°W is compared to the energy density at .02° cph of our latitude band 2 (Fig. 8). To obtain the frequency spectrum the frequency-wavenumber spectrum is integrated over all wavenumbers. At .02 cph, the energy density is ∿118 $(m/sec)^2/cph$, whereas Halpern finds a value of ∿120 $(m/sec)^2/cph$. The agreement between the two values is good. The distribution of energy density in the overlapping frequency range of the two studies is different. Halpern's spectrum is red in this range whereas my results reveal a white spectrum. Figure 10 shows a comparison of the two spectra. Values for the Halpern spectrum were read directly from his spectral plots.

IV. Summary and Conclusions

The principal findings of this study are:

1) The maximum energy density levels of the meridional component of the satellite estimated 900 mb wind occur at low wavenumbers over a broad spectrum of frequencies in the Equatorial Pacific Ocean.

2) It is difficult to investigate low frequency spectral structure with the satellite cloud drift data. Aliasing from high frequency and high wavenumber disturbances is a major problem, confusing the low frequency spectra.

3) Investigation of the high frequency-high wavenumber structure of the equatorial meridional wind field using satellite cloud drift data is difficult due to the general shortage of reliable

data and the uneven sampling interval of the satellite system necessitated by proper level cloud occurrence frequencies, daylight hours, avoidance of high level clouds and low confidence in both cloud height and velocity estimates. This results in statistically unreliable conclusions.

4) There was no clear indication of a distinct 4-day signal in the meridional wind component in the two southerly latitude bands studied, although the equatorial band does show some activity at 4 and 5 days at low wavenumbers (Fig. 9).

5) High frequency energy seems to be lower in the immediate vicinity of the equator (band 3) than in other latitude bands.

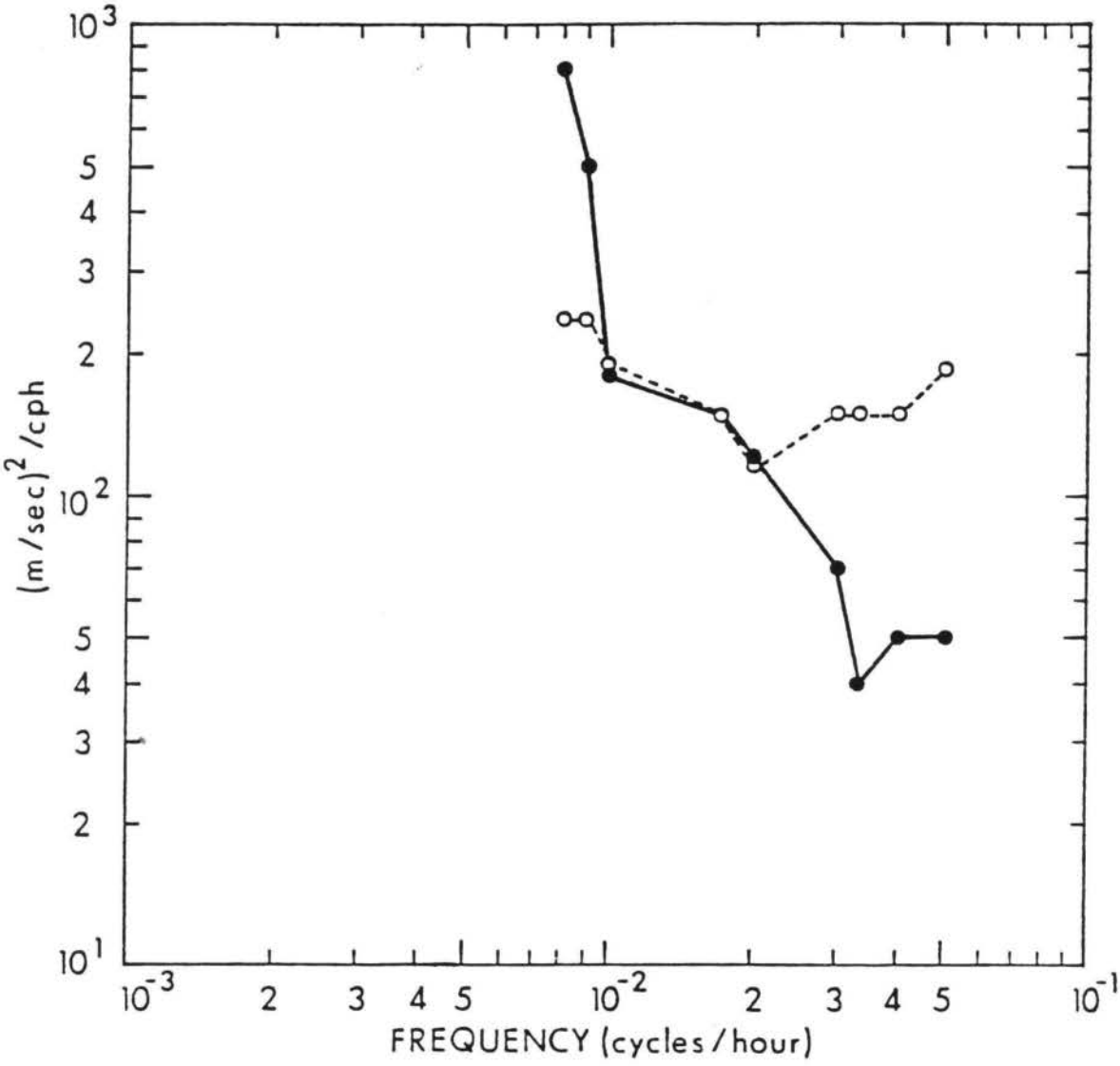

Fig. 10. Comparison of the Halpern (1978) spectrum (solid line) with our spectrum for the overlapping frequency range of the two studies.

APPENDIX

Statistical Significance of the Results

A1. Variance of a Product

In the estimation of the autocovariance function $R(\eta,\tau)$ the products of velocity component values at different times and longitudes are summed. Let v_1 and v_2 be two such individual velocity component values, and let us assume that they are distributed as bivariate normal random variables with each having the same mean m, the same variance σ^2 and correlation coefficient ρ. Thus, the probability density distribution is given by

$$f(v_1,v_2) = \frac{(1-\rho^2)^{-1/2}}{2\pi\sigma^2} \exp\left\{-\lambda\left[(v_1-m)^2 - 2\rho(v_1-m)(v_2-m) + (v_2-m)^2\right]\right\} \tag{A1-1}$$

where

$$\lambda = \frac{1}{2\sigma^2(1-\rho^2)}$$

We now wish to consider the distribution of the quantity $p = v_1 v_2$. If $m \neq 0$ it is difficult and perhaps not feasible to obtain the distribution function f(p) from (A1-1) in closed form, but satisfactory error estimates can be based on the mean and variance of this distribution, which are readily obtained. The nth moment of f(p) is given by

$$\mu_n = \int_{-\infty}^{\infty}\int_{-\infty}^{\infty} v_1^n v_2^n f(v_1,v_2)\,dv_1\,dv_2 \tag{A1-2}$$

The above integrals are readily evaluated, for the cases n = 1 and n = 2, with the help of formulas 3.225.3 and 3.271 of Ryzhik and Gradstein (1957), with the result

$$\mu_1 = \rho\sigma^2 + m^2$$

$$\mu_2 = (1 + 2\rho^2)\sigma^4 + 2(1+2\rho)m^2\sigma^2 + m^4 . \qquad \text{(A1-3)}$$

The variance of p about its mean value is given by

$$\sigma_p^2 = \mu_2 - \mu_1^2 = (1+\rho^2)\sigma^4 + 2(1+\rho)m^2\sigma^2 \qquad \text{(A1-4)}$$

It is convenient to find an expression for this variance which does not contain the unknown correlation coefficient ρ. It is possible to estimate reasonable values of the common mean and variance of the individual v values, but the correlation coefficient between pairs of values depends on their proximity in longitude and time. Now p is an estimate of R, which is the true value of the desired autocovariance function at a particular longitude separation and time lag. Eliminating ρ between (A1-3) and (A1-4) gives

$$\sigma_p^2 = \mu_1^2 + \sigma^4 + 2m^2\sigma^2 - m^4 \qquad \text{(A1-5)}$$

in which the unknown μ_1 can be approximated by substituting for it the corresponding estimated value of the autocovariance function. Such an approximation is usually referred to as large sample theory.

A2. Variance of the Estimated Autocovariance Values

These values are just the averages of a number n of products p where n is the number of products whose corresponding longitude separations and time lags fall within certain limits. The actual v values will occur at widely varying longitudes and times, and there is no convenient way to estimate the correlations between the individual p values. The easiest procedure is to assume that the p values are independent, and this assumption is hereby made. The variance of each estimate of R is then just

$$\sigma_R^2 = \sigma_p^2 / n \qquad \text{(A2-1)}$$

A3. Variance of the Estimated Spectrum Values

Here we shall similarly assume that the individual estimates of R at the different longitude separations and time lags are independent. Then, as is seen from formula (III-11), each S value is just a linear combination of the R estimates. Thus, its variance is just the sum of the σ_R^2 values weighted by the square of each coefficient of the linear combination. The result for each value $S(\kappa,\sigma)$ of spectral density for longitudinal wave number $\kappa = k\Delta\kappa$ and frequency $\sigma = j\Delta\sigma$, is

$$\sigma_{S_{jk}}^2 = \sum_{p=-\ell}^{\ell} \sum_{q=-m}^{m} Q_{jkpq}\, \sigma_{R_{pq}}^2 \qquad \text{(A3-1)}$$

where σ_{Rpq}^2 are the variances of the individual estimates of $R(\eta,\tau)$ at longitude separation $\eta = p\Delta\eta$ and time lag $\tau = q\Delta\tau$. Here, Q_{jkpq} is given by

$$\Delta\eta^2 \Delta\tau^2 \cos^2\left[\frac{2\pi jp}{2\ell+1} + \frac{2\pi kq}{2m+1}\right] \tag{A3-2}$$

where ℓ, m are as defined in (III-7).

The intracacies of the quadruply-subscripted Q hampers understanding of the error dependence on the fundamental parameters of the problem. Also, many computations are required. For these reasons it is convenient to define a mean variance of the spectral estimates,

$$\sigma_s^2 \equiv \frac{1}{2\ell+1}\frac{1}{2m+1}\sum_{j=-\ell}^{\ell}\sum_{k=-m}^{m}\sigma_{S_{jk}}^2 = \sum_{p}\sum_{q} Q_{pq}\,\sigma_{R_{pq}}^2 \tag{A3-3}$$

where

$$Q_{pq} \equiv \frac{1}{2\ell+1}\frac{1}{2m+1}\sum_{j=-\ell}^{\ell}\sum_{k=-m}^{m} Q_{jkpq} \tag{A3-4}$$

Thus,

$$Q_{00} = \Delta\eta^2 \Delta\tau^2$$

$$Q_{pq} = \tfrac{1}{2}\Delta\eta^2 \Delta\tau^2 \;; \quad p^2+q^2 > 0. \tag{A3-5}$$

The value σ_s^2 is what is indicated as the mean variance of the spectral estimates.

REFERENCES

Barnett, T.P., 1977: The principal time and space scales of the Pacific trade wind fields. J. Atmos. Sci., 34, 221-236.

Green, R., G. Hughes, C. Novak and R. Schreitz, 1975: The automatic extraction of wind estimates from VISSR data. Central Processing and Analysis of Geostationary Satellite Data, C.L. Bristor, ed., NOAA Tech. Mem. NESS 64, National Oceanic and Atmospheric Administration, Washington, D.C., 94-110.

Groves, G.W., 1956: Periodic variation of sea level induced by equatorial waves in the easterlies. Deep-Sea Res., 3(4), 248-252.

Groves, G.W. and Motoyasu Miyata, 1967: On weather-induced long waves in the equatorial Pacific. J. Mar. Res., 25, 115-128.

Halpern, D., 1978: Comparison of low-level cloud motion vectors and moored buoy winds. J. Appl. Meteorol., 17, 1886-1871.

Munk, W., F. Snodgrass and F. Gilbert, 1964: Long waves on the continental shelf: an experiment to separate trapped and leaky modes. J. Fluid Mech., 20, 529_554.

Ryzhik, I.M. and I.S. Gradstein, 1963: Tables of Series, Products, and Integrals. Veb Deutscher Verlag der Wissenschaften, Berlin, 438 pp.

Suomi, V.E. (Principal Investigator), 1975: Man-computer interactive data access system (MIDAS). Final Report Contract NASS-23296, University of Wisconsin, Madison.

Wallace, J.M., 1971: Spectral studies of tropospheric wave disturbances in the tropical western Pacific. Rev. of Geo. and Space Physics, 9, 557-612.

Wyrtki, K. and G. Meyers, 1976: The trade wind field over the Pacific Ocean. J. Appl. Meteor., 15, 698-704.

Young, M.T., 1975: The GOES wind operation, Central Processing and Analysis of Geostationary Satellite Data, C.L. Bristor, ed., NOAA Tech. Mem. NESS 64, National Oceanic and Atmospheric Administration, Washington, D.C., 111-121.

Young, M.T., R.C. Doolittle and L.M. Mace, 1972: Operational procedures for estimating wind vectors from geostationary satellite data. NOAA Tech. Mem. NESS 39, National Oceanic and Atmospheric Administration, Washington, D.C.